CHAPTER 5

Results and Discussion

5.1 Physical Observations

The weight changes, color and response of the samples when a bar magnet is brought near is provided in Table 5.1. There is a slight weight gain in ZIO-1, which could be due to the precipitation of iron oxides in the zeolite matrix, while weight loss was observed for the other samples. The weight of exchanged, but unprecipitated zeolite was also recorded. Infact, this sample had a very slight weight loss of 0.72%, which very likely could be due to some samples that were lost during washing and transfer between containers. More interestingly, 83-84% loss of weight was recorded for samples ZIO-3, ZIO-4 and ZIO-5. This is attributed to the action of highly concentrated NaOH which destroyed the zeolite powders. The remaining product is believed to constitute mostly of iron oxides.

To test this assumption, 1g of zeolite Y powder was added to a 25 ml solution of 12.5M NaOH and left for several hours. Upon observation 2 hours later, the white powder of the zeolite had dissolved completely into the solution, leading us to conclude that the extremely high pH of the alkali had not only caused the zeolite to undergo amorphization, but to completely dissolute (as will be shown in EDS results in Section 5.2 and XRD phase studies in Section 5.3).

The colors of the precipitated products range from a deep orange to reddish brown, according to the increasing molarity of the NaOH solution. ZIO-1 and ZIO-2 showed no response to a bar magnet while the other three samples were attracted to the magnet when it was brought near, indicating the presence of a magnetic oxide phase.

Table 5.1: Compilation of physical characteristics of samples before being subjected to further characterization.

Sample	Weight of zeolite (g)	Weight of product (g)	Weight changes (%)	Color of dried precipitate	Response to bar magnet
z-Fe	1.01596	1.00865	-0.72	Light green	No
ZIO-1	1.00016	1.07400	6.88	Orange	No
ZIO-2	1.01965	0.84606	-17.0	Orange	No
ZIO-3	1.03570	0.17424	-83.2	Light brown	Yes
ZIO-4	1.01736	0.16887	-83.4	Brown	Yes
ZIO-5	1.07850	0.17210	-84.0	Reddish brown	Yes

5.2 Elemental Composition

Analysis of the ZIO systems by the semi-quantitative method of EDS was used instead of the quantitative method of x-ray fluorescence spectroscopy (XRF) because the weight of the synthesis product was between 0.17 g to 1.07 g (Table 5.1), which was insufficient to produce samples for XRF testing. Pure zeolite powder was characterized by XRF, and the results are furnished in Appendix 1.

As can be seen in Table 5.2, results from EDS show that the relative contents of iron increases as well as that of sodium decreases in the ZIO samples compared with the pure untreated zeolite Y. The pure zeolite does not contain any detectable iron. The exchanged zeolite (z-Fe) sample shows the presence of a significant amount of iron and quite a large decrease of sodium. This indicates the successful uptake of iron cations from the ion-exchange procedure.

The precipitated zeolite samples (ZIO-1 to ZIO-5) show increasing iron content while its sodium concentration is relatively high. This is attributed to the readsorption of Na ions from the NaOH solution used for oxidation, in order to balance the zeolite structure after Fe(II) ions are precipitated.

A decrease of 6.2 wt. % of sodium content is detected in the z-Fe sample. For a basis of 100 g sample, this translates to a loss of about 0.27 moles of Na^+. There is also a matching uptake of 5.5 wt. % of iron in the system, corresponding to 0.1 moles of Fe^{2+}. These figures are very close to the assumption that one Fe^{2+} cation is replacing every two Na^+ cations in order to balance the zeolite electronic structure (as mentioned previously in Section 2.1). Minor quantities of Fe^{3+} arising from oxidation of Fe^{2+} can affect the Na^+-Fe^{2+} exchange ratio.

Table 5.2: Elemental composition and Si:Al molar ratio of various treated zeolite samples (wt. %)

Element	Pure zeolite Y	Zeolite-Fe(II) samples treated with various concentrations of NaOH					
		z-Fe	ZIO-1	ZIO-2	ZIO-3	ZIO-4	ZIO-5
Fe	-	5.5	4.9	5.7	28.5	43.2	50.3
Na	9.3	3.1	9.3	7.9	6.7	13.2	5.3
Si	28.5	22.8	27.0	23.1	11.9	1.8	2.6
Al	10.9	9.6	10.4	9.1	5.1	0.4	0.5
O	51.3	59.0	48.4	54.2	47.5	41.2	40.8
Ca	0	0	0	0	0.3	0.2	0.5
Total Wt. %	100.0	100.0	100.0	100.0	100.0	100.0	100.0
Si:Al Molar Ratio	2.5	2.3	2.5	2.4	2.2	4.3	5.0

An apparent decrease of the relative contents of silicon and aluminum were also observed, leading to the belief that the structure of the zeolite is being affected by the chemical interactions. However, a simple calculation of the mole ratio between silicon and aluminum for the pure zeolite gave a value of 2.5, which is in reasonable agreement with the ZIO-1, ZIO-2 and ZIO-3 samples. For ZIO-4 and ZIO-5, Si:Al mole ratios of 4.3 and 5.0 respectively were obtained, differing up to 200% from the original mole ratio in the pure zeolite Y. This is attributed to the intense concentration of the NaOH, which not only accelerated the iron oxide formation, but also affected the original crystal structure of the zeolite.

The calcium trace content that was registered on the composition of ZIO-4 and ZIO-5 is believed to have originated from the zeolite. An elemental analysis of the pure zeolite using XRF (Appendix 1) shows that it contains 0.15 wt. % calcium oxide.

5.3 Phase and Crystal Structure

X-ray diffraction spectra (the as-measured scans taken directly from the measuring instrument) of the zeolite-iron oxide (ZIO) precipitated samples are shown in Fig. 5.1. Patterns (b) to (f) in the graph are the patterns of ZIO-1 to ZIO-5 respectively. These are compared with the diffraction pattern of the pure zeolite Na-Y powder shown in Fig. 5.1 (a). The full diffraction patterns are provided in Appendix 3.

It is obvious from Fig. 5.1 that the spectra for ZIO-1 and ZIO-2 are similar to that of the pure zeolite, while the pattern of ZIO-3 retains only a number of peaks. An evolution of new peaks with a broader width is also apparent in this sample. These peaks become more pronounced in samples ZIO-4 and ZIO-5. This indicates that the ZIO samples are transforming from a phase similar to the pure zeolite phase and structure to a new phase, possibly the desired iron oxide phase, due to the precipitation procedure and the dissolution of zeolites at high concentrations of NaOH.

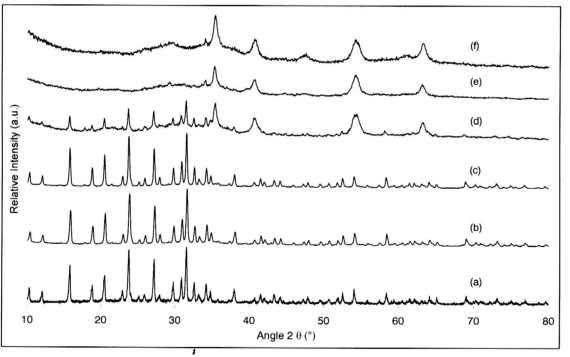

Fig. 5.1: Diffraction spectra of the precipitated zeolite-iron oxide (ZIO) samples [patterns (b) to (f)] compared with the pattern of pure zeolite Na-Y (a).

Very few zeolite peaks were observed on the patterns of ZIO-4 and ZIO-5, suggesting that the crystal structure of zeolite was destroyed through the precipitation procedure. A separate test on the effect of highly concentrated NaOH on zeolite powder was conducted. In this simple test, about 1g of zeolite powder was added to a 25 ml of 12.5M NaOH solution at room temperature and left for 10 hours. After a sufficient amount of time had elapsed, it was noticed that the white zeolite powder had been completely dissolved into the base, leaving a clear solution.

After subtracting the background 'noise' from the measured scan of ZIO-4 and ZIO-5, the patterns shown in Fig. 5.2 were obtained. The phase identification process involved a search and match operation of the peak positions of these two ZIO samples with the diffraction patterns of standard reference materials from the International Centre for Diffraction Data (ICDD) database (refer to Section 4.1.2) and eliminating all non-ferrous oxide matches. Due to the low number of peaks which usually exist for nanometer-sized powder samples, the usual method of identifying a compound by 3 peaks [71] was not able to be carried out. A list of possible phase and compounds was narrowed down only to magnetic iron oxide phases such as gamma iron oxide (maghemite) and remaining unidentified peaks were assigned to non-magnetic iron oxide phases such as alpha iron oxide (hematite). Furthermore, the standard reference compounds are usually measured on perfect single crystal samples.

It was found that the ZIO samples are composed of a mixture of gamma iron oxide (maghemite) and alpha iron oxide (hematite). This is because the peaks at angle 2θ of 35.4° and 63.1° belong to the planes (311) and (440) respectively of gamma iron oxide (ICDD PDF card no. 39-1346), while the peaks at 40.7° and 54.2° correspond to planes (113) and (116) respectively of alpha iron oxide (ICDD PDF card no. 03-0800). The peak at 47.5° originates from the (200) plane of gamma iron oxide hydrate (γ-$Fe_2O_3 \cdot H_2O$) (ICDD PDF card no. 02-0127).

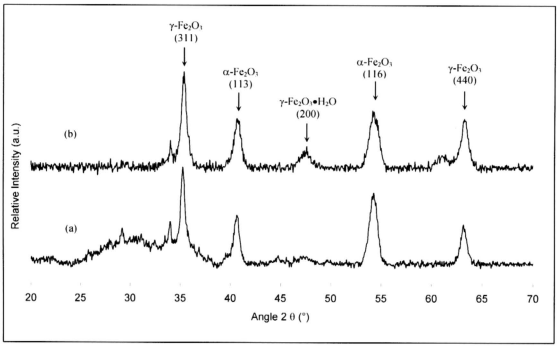

Fig. 5.2: The diffraction patterns of (a) ZIO-4 and (b) ZIO-5, after subtracting the background contribution.

A comparison of d-spacing values between standard reference material patterns from ICDD PDF (Appendix 2A, 2B and 2C) and the ZIO-5 sample is shown in Table 5.3. The d-spacings are calculated from Bragg's Law of $n\lambda = 2\ d\ \sin\theta$, where $n = 1$ and λ is the wavelength of Cu K-α rays (1.54056 Å).

Table 5.3: Comparison of peak positions and d-spacings between standard reference materials and ZIO-5

Miller indices (h k l)	**Phase**	**Standard reference**		**ZIO-5**	
		2θ (°)	**d-spacing (Å)**	**2θ (°)**	**d-spacing (Å)**
3 1 1	γ-Fe_2O_3	35.661	2.516	35.380	2.535
1 1 3	α-Fe_2O_3	40.832	2.208	40.715	2.214
2 0 0	γ-Fe_2O_3•H_2O	47.086	1.928	47.514	1.912
1 1 6	α-Fe_2O_3	53.935	1.699	54.218	1.690
4 4 0	γ-Fe_2O_3	62.983	1.475	63.133	1.471

The peaks also show noticeable broadening that correlates to the fine particle size. Table 5.4 shows a tabulation of the average crystallite size in ZIO-5 that was obtained by application of Scherrer's equation (refer Section 4.1.2). The spectra for ZIO-1 and ZIO-2 consist of a combination of zeolite and iron oxide peaks, which are difficult to isolate, whereas ZIO-3 and ZIO-4 have remanent amorphous zeolite peaks, making analysis of the peak heights difficult. ZIO-5 was chosen for iron oxide crystallite size analysis as it could be ascertained that the zeolite phase was destroyed (the test to demonstrate the dissolution of zeolite was mentioned in Section 5.1), leaving only iron oxide compounds in the sample.

The full width at half maximum (β_{sample}) values obtained for seven peaks from ZIO-5 were determined from a profile fitting software, ProFit. The results are attached in Appendix 4. The program decomposes a powder diffraction pattern into its constituent Bragg reflections, yielding defining parameters of each reflection, such as its position, intensity, breadth and shape. In Scherrer's equation, the β value is inversely proportional to crystallite size, meaning that a large β value corresponds to a very fine crystallite size. The diffractometer itself also contributes a minor broadening effect that is recorded during measurement of a sample. A standard calibration material lanthanum hexaboride (LaB_6), (SRM660), has been used for the instrumental broadening measurement, and a standard value of $\beta_{instrument}$ of 0.15° is subtracted from each value of β_{sample} to yield the corrected values ($\beta_{corrected}$).

Table 5.4: Estimation of crystallite sizes of zeolite-iron oxide from ZIO-5 calculated using Scherrer's equation.

Angle 2θ (°)	Peak broadening in terms of FWHM (radians)		Crystallite size, D (nm)
	β_{sample}	$\beta_{corrected}$	
35.3013	0.0100	0.0074	19.7
40.6640	0.0133	0.0106	13.9
47.4134	0.0230	0.0204	7.4
54.2388	0.0201	0.0175	8.9
60.9506	0.0100	0.0074	21.7
63.2299	0.0138	0.0112	14.5
88.0632	0.0272	0.0246	7.9
		Average crystallite size:	**13.4**

5.4 Particle Morphology

The changes in morphology of the ZIO samples can be followed from the SEM micrographs shown in Fig. 5.3. As can be seen in Fig. 5.3(a), the discrete and hexagonal shape of pure zeolites appear to have broken down and replaced by the magnetic iron oxide (sample ZIO-5) with a cluster-like appearance as seen in Fig. 5.3 (f). Fig. 5.3 (b) to Fig. 5.3 (e) shows the intermediate between these two extreme conditions. The cluster morphology seen in ZIO-5 is completely different to the acicular iron oxide that was obtained by free precipitation (the sample is labeled ZIO-0), without any constraining matrix (seen in Fig. 5.4). We can surmise that even though the zeolite structure appears to have dissolved in the high pH of the NaOH, the formation of the iron oxide preceded this occurrence in order for the clusters to develop. Very fine equiaxed crystallites about 25nm in uniform size were observed from TEM images of the ZIO-3 and ZIO-5 dispersions as shown in Fig. 5.5(a) and 5.5(b) respectively. However, a mixture of acicular and circular nanostructures was observed from the dispersions of the ZIO-1, ZIO-2 and ZIO-4 samples [Figs. 5.5(c), 5.5(d) and 5.5(e)].

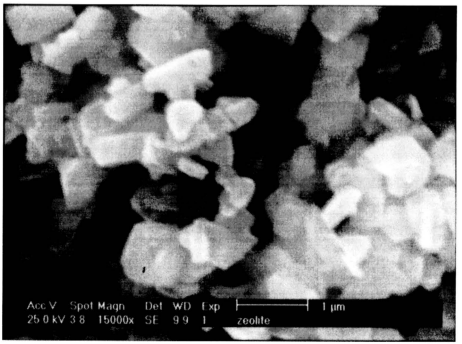

Fig. 5.3(a): SEM image of pure zeolite powder.

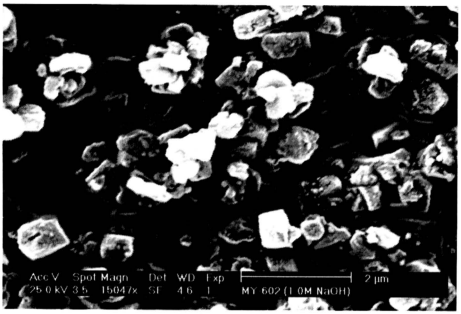

Fig. 5.3(b): SEM image of ZIO-1.

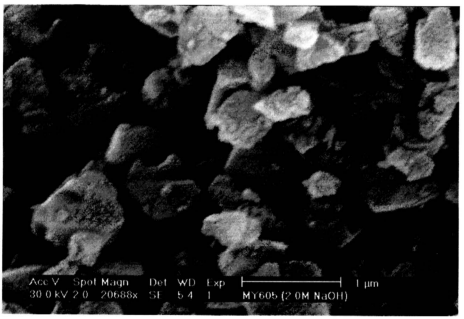

Fig. 5.3(c): SEM image of ZIO-2.

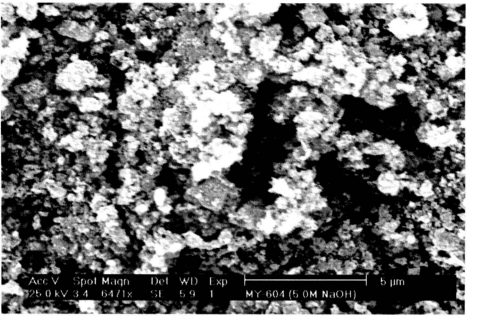

Fig. 5.3(d): SEM image of ZIO-3.

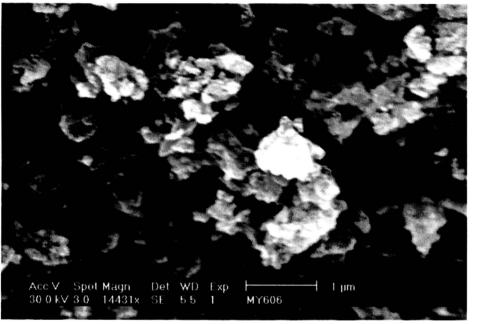

Fig. 5.3(e): SEM image of ZIO-4.

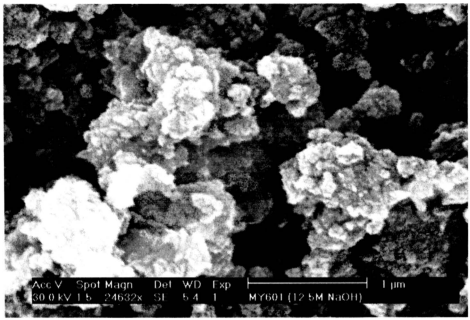

Fig. 5.3(f): SEM image of ZIO-5.

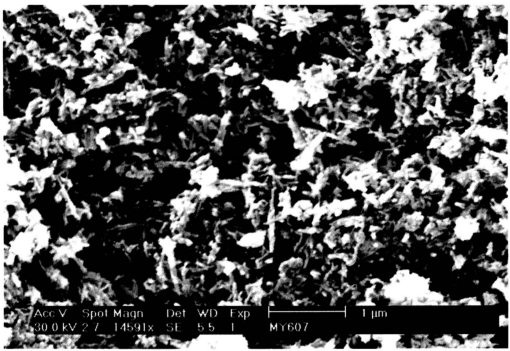

Fig. 5.4: The surface morphology of ZIO-0 obtained from free precipitation without zeolite constraining effect, as observed under SEM.

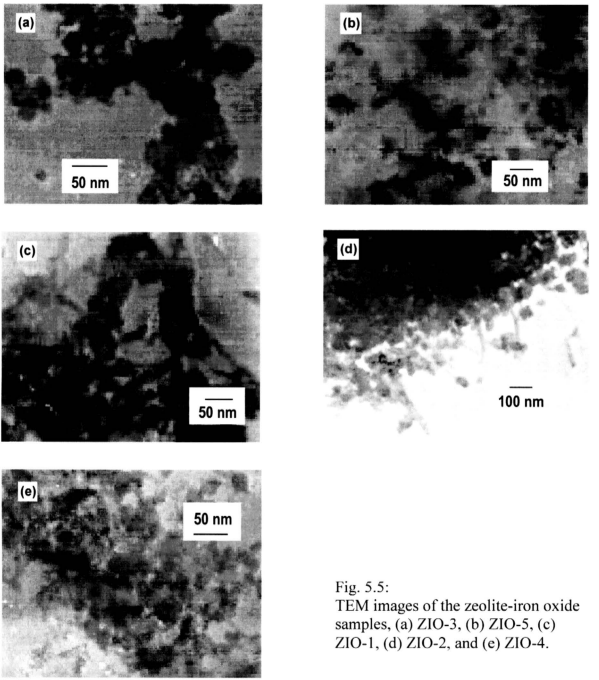

Fig. 5.5:
TEM images of the zeolite-iron oxide samples, (a) ZIO-3, (b) ZIO-5, (c) ZIO-1, (d) ZIO-2, and (e) ZIO-4.

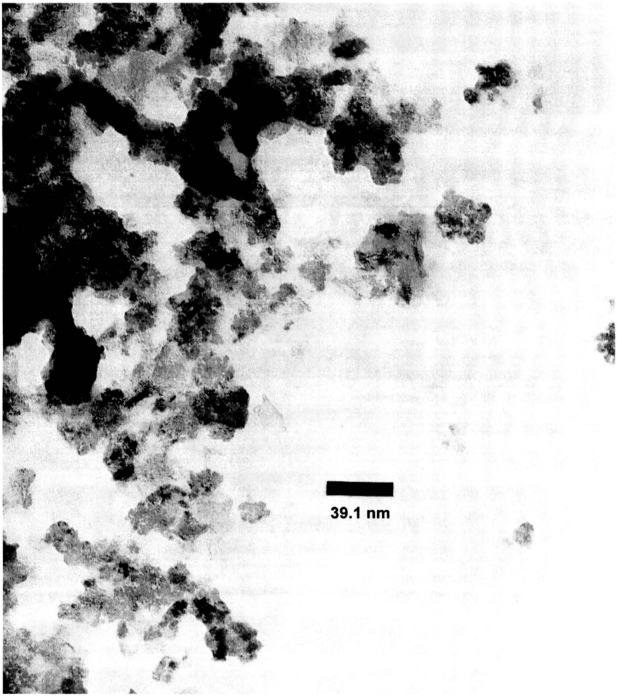

Fig. 5.6: The ZIO-5 system as seen under TEM.

5.5 Response to Magnetic Field

The behavior of all ZIO samples under the influence of an applied magnetic field that alternated from a maximum of 10 kOe to a minimum of -10 kOe was measured at room temperature (T = 298 K) and summed up in Table 5.5.

Table 5.5: Summary of magnetic properties of ZIO samples.

Sample	$M_{10\ kOe}$ (emu/g)	M_r (emu/g)	H_c (kOe)	Presence of hysteresis
ZIO-0	32.47	8.642	0.204	Yes
ZIO-1	0.360	0.069	0.056	Yes
ZIO-2	1.205	0.118	0.011	No
ZIO-3	10.16	1.041	0.014	No
ZIO-4	9.669	1.097	0.015	No
ZIO-5	6.733	0.362	0.007	No

The magnetization versus applied field graphs of samples ZIO-2 [seen in Fig. 5.7(b)], ZIO-3, ZIO-4 and ZIO-5 (all shown in Fig. 5.8) pass through the origins of the graphs, and no observable remanent magnetization (M_r) and coercivity (H_c) can be seen. The curve for ZIO-1 [Fig. 5.7(a)] displays a slight hysteresis. The magnetization curve for ZIO-0, the iron oxide sample that was precipitated with 10.0 M NaOH without the presence of zeolite constraints (similar to ZIO-4), show a clear hysteresis loop as seen in Fig. 5.9. Its magnetization value at the maximum applied field of 10 kOe (M_{10kOe}) is more than 300% greater than that of ZIO-4.

When the particles are characterized by a non-uniform size distribution, the major contribution to the slope near zero applied field (H=0) comes from the largest particles. Thus, we can arrive at a least upper bound for this magnetic size [40]. By taking into consideration the major component of the samples are maghemite, and that their saturation magnetization (M_s) correspond to that of the bulk material (74 emu/g), the least upper bound for the 'magnetic' size of these particles is given by:

$$d_{mag} = \left[\frac{18kT}{\pi} \frac{(dM/dH)_{H=0}}{\rho M_s^2} \right]^{1/3}$$

where ρ is the density of bulk maghemite (5.07g/cm^3). The Boltzmann constant, *k*, is taken as 1.38 x 10^{-16} erg/K, in agreement with the other cgs units used here. The absolute temperature, *T*, is set at 298K.

The 'magnetic' sizes in Table 5.6 are calculated for all four samples that exhibited superparamagnetic behavior. These results show that the 'magnetic size' of the particles varies with different NaOH concentrations.

Table 5.6: 'Magnetic' size of the particles.

Sample	$(dM/dH)_{H=0}$, **(emu/g Oe)**	d_{mag}, **(nm)**
ZIO-2	7.17 x 10^{-3}	3.933
ZIO-3	6.20 x 10^{-2}	8.073
ZIO-4	7.05 x 10^{-2}	8.426
ZIO-5	4.37 x 10^{-2}	7.185

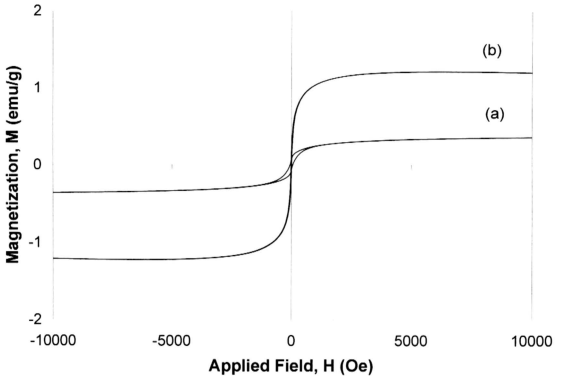

Fig. 5.7: The magnetization curves of (a) ZIO-1 and (b) ZIO-2.

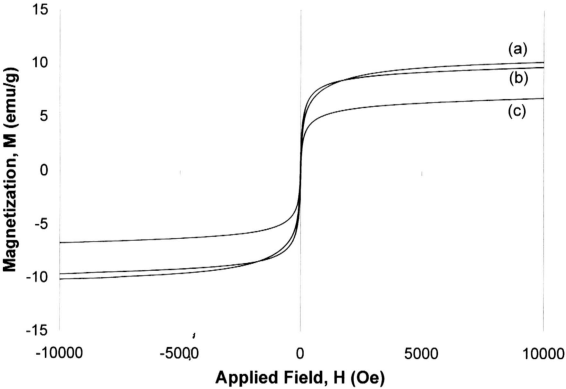

Fig. 5.8: Magnetization curves of (a) ZIO-3, (b) ZIO-4 and (c) ZIO-5.

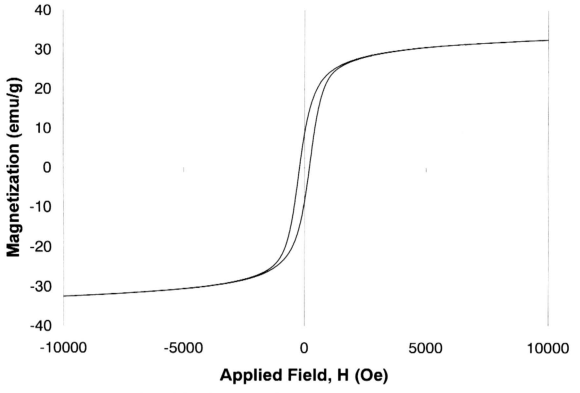

Fig. 5.9: The magnetization curve of ZIO-0.

The gradient of the magnetization curves near H=0 increases in the order: ZIO-2, ZIO-5, ZIO-3 and ZIO-4. The steeper gradient indicates a larger increase of magnetization, which is accompanied by larger particle size. The specific saturation magnetization is also influenced by specific surface area and particle morphology [19]. The magnetization versus applied field curves in Fig. 5.7 shows that ZIO-3 has the highest magnetization value of 10.16 emu/g, but none of the samples achieved saturation at 10 kOe. The M_s values could not be ascertained because the instrument is limited to a maximum applied field of 10 kOe.

The oxidation process using highly concentrated NaOH solutions facilitated the transformation of the iron (II) cations into the ferrimagnetic γ-Fe_2O_3 phase and the weakly-ferromagnetic α- Fe_2O_3 phase. It appears that more of the non-magnetic phase is being formed as the concentration of NaOH is increased to 10.0M and 12.5M, causing a drop in the magnetization at the maximum applied field.

The explanation for the curves without hysteresis obtained in Fig. 5.8 can be approached from the particle size aspect. In bulk form, maghemite is a ferrimagnet with a Neel temperature well above 600°C. This means that above that temperature, relaxation of the magnetic moments occur, because thermal excitation causes the moments to fluctuate in random directions. As mentioned before, magnetic properties such as coercivity, blocking temperature, saturation magnetization and remanent field are a function of the particle size, shape and surface chemistry [12-14]. When the particle size is sufficiently small, ferrimagnetic materials lose their magnetization below the Neel temperature and become superparamagnetic. The material therefore no longer exhibits any hysteresis. This is due to the fact that magnetic particles below a certain critical size cannot support more than one domain. The magnetization vector thus becomes unstable in this size range and begins to wander in a thermally activated manner analogous to Brownian movement. The magnetic anisotropy energy of a particle is proportional to its volume. When the volume is small enough, the magnetic energy of the particle approaches its thermal energy kT. The magnetization vector fluctuates in the same way as in a classical paramagnetic gas [72].

5.6 Pore Size Measurements

The adsorption isotherm of the pure zeolite Y powder is shown in Fig. 5.10. The shape of the isotherm is characteristic of materials possessing a high surface area. The specific surface area, as calculated using the B.E.T. method, is 615.0 m^2/g. The adsorption isotherm of the zeolite sample exchanged with Fe^{2+} cations also show a similar curve, as seen in Fig. 5.11 (a), with little change in specific surface area (617.5 m^2/g). However, an increase in specific surface area of 26% was recorded in the zeolite sample precipitated with 2.0 M NaOH (ZIO-2), seen in Fig. 5.11 (b). This particular zeolite sample had a specific surface area of 784.8 m^2/g. It was chosen instead of the other precipitated samples because the integrity of the zeolite structure was still intact after the precipitation procedure, and it also exhibited superparamagnetic behavior. The increase in specific surface area in ZIO-2 strongly suggests that fine particles of iron oxide were formed within the internal pores, hence adding to the total surface area.

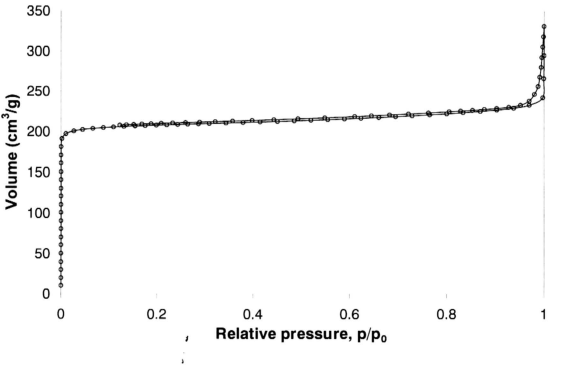

Fig. 5.10: Adsorption-desorption isotherm of pure zeolite Y powder

Due to the microporous nature of the zeolite system, and the apparent formation of iron oxide within the zeolite pores, the size of these particles in the ZIO-2 system can be calculated by using the formula

$$l = \frac{6}{\rho S} \qquad \ldots\ldots \quad \text{(Equation 5.1)}$$

where l is the length of the cube, ρ is the density of maghemite (5.07 g/cm^3) and S is the specific surface area. Particles of about 7.1 nm are obtained from the calculation. This value is in the same range of the magnetic size obtained from AGM measurements, if magnetically 'dead' surface layer of about 1.5 nm exists.

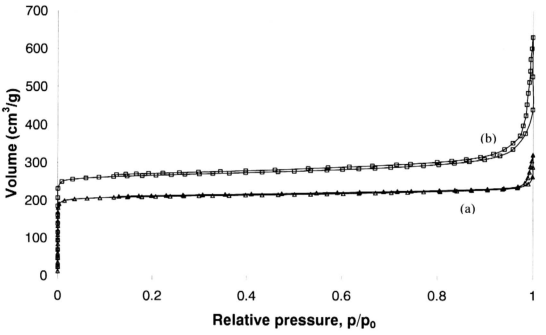

Fig. 5.11: Adsorption-desorption isotherm of (a) Fe(II)-exchanged zeolite Y and (b) ZIO-2.